Supplementary information: Band structure of CuMnAs probed by optical and photoemission spectroscopy

M. Veis, J. Minár, G. Steciuk, L. Palatinus, C. Rinaldi, M. Cantoni, D. Kriegner, K.K. Tikuišis, J. Hamrle, M. Zahradnik, R. Antoš, J. Železný, L. Šmejkal, X. Marti, P. Wadley, R.P. Campion, C. Frontera, K. Uhlířová, T. Duchoň, P. Kužel, V. Novák, T. Jungwirth, and K. Výborný

I. X-RAY CHARACTERISATION

X-ray scattering and diffraction measurements were used to check the thin-film thickness and the tetragonal structure in Fig. 1 of the main text. The obtained parameters, described in detail below, are summarised in Tab. I here, and can be compared to values from Tab. I in the main text. We first describe the X-ray reflectivity analysis which yields the film thickness and roughness of the sample which we compare to the analysis of ellipsometric measurements. After that we turn to the structural characterization complementary to the PEDT data presented in the main text.

A. X-ray reflectivity analysis of the film thickness

X-ray reflectometry (XRR) was recorded with a Rigaku Smartlab rotating anode system using monochromatic X-ray photons with $CuK_{\alpha 1}$ wavelength. Since the refractive index of materials is below unity total external reflection occurs under small incidence angles. Above the critical angle where the X-rays penetrate the film material, Kiessig fringes due to the interference of X-rays reflected at the top and bottom interface of the thin film correspond to the film thickness and can be modeled by the Parrat formalism.[2] Experimental data in comparison with simulations are shown in Fig. 1. The simulations yield a total film thickness of 22.7 nm and a surface and interface roughness of around 0.4 nm. We note that the X-ray reflectivity analysis was performed after the sample was exposed to air for longer time and therefore some oxide, present on the surface as discussed below, was included in the XRR simulations. For comparison with values determined by ellipsometry (see main text and the discussion in Sec. II below) we therefore use the total thickness. Given that different pieces of wafer were used for individual measurements (i.e. the same growth run but different storage conditions), we find an excellent agreement.

B. X-ray diffraction analysis of the tetragonal structure

Due to large penetration depth of x-ray photons, X-ray diffraction (XRD) probes the full film depth including the substrate below — the advantage being that no sample preparation is required for XRD measurements, which therefore naturally complement the PEDT data in the main text. Despite certain other advantages, PEDT requires a complex specimen

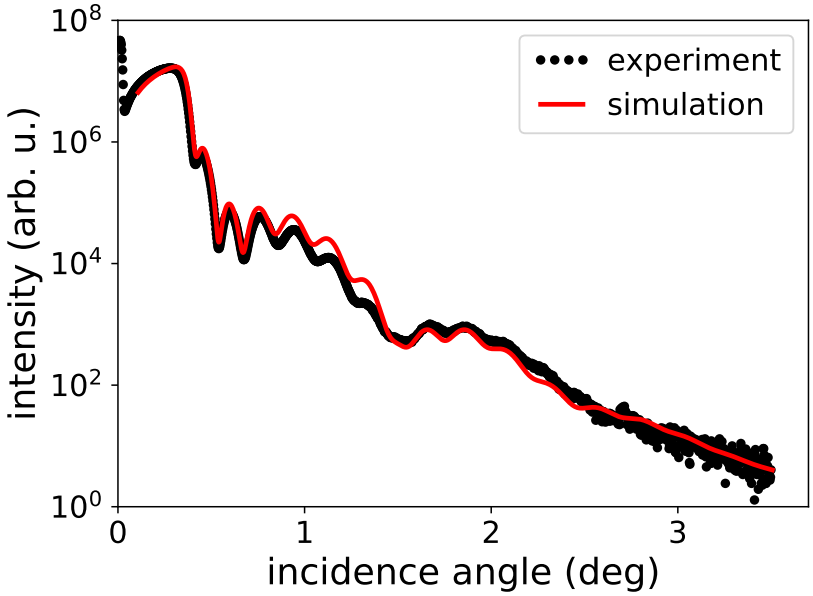

FIG. 1. X-ray reflectivity data and simulations of the sample investigated by ellipsometry.

description:	CuMnAs/GaAs	CuMnAs/GaP
	Ref. 1	this work
a [Å]	3.820(10)	3.853(1)
c [Å]	6.318(10)	6.276(1)
z/c for S^2	0.265(1)	0.259(1)
z/c for S^3	0.670(3)	0.664(1)
ADP [Å^2]	-	0.028(3)
R_B	-	3.97%

TABLE I. Structural parameters of CuMnAs thin films grown on GaP(001) and GaAs(001) substrates. The latter were converted from values published in Ref. 1.

preparation. Further, XRD has a higher precision for lattice parameter measurements; thin films grown on GaP(001) yield lattice parameters specified in Tab. I. These measurements were performed using the aforementioned Rigaku Smartlab rotating anode system using monochromatic X-ray photons with $CuK_{\alpha 1}$ and a linear detector.

The determination of the atomic structure of the thin films was performed as described in detail in Ref. 1. For that purpose we used a Bruker D8-Discover diffractometer equipped with

a Våntec-500 area detector. The difference between lattice parameter of CuMnAs (~ 6.3 Å) and GaP (~ 5.45 Å) warrants that no significant overlapping between diffraction peaks from substrate and from film takes place. The total number of diffraction peaks measured was 44. The number of observable diffractions is therefore considerable lower as in the PEDT data in the main text. This is compensated by easier modeling which in total only requires 5 structural parameters as opposed to observables (27 independent reflections) and a single one overall factor. The structural refinement includes an overall temperature factor, the two z/c positions of S_2 and S_3, reported in the Tab. I. The shorter range in Q-space available for the long wavelength of Cu-Kα (in comparison with electrons), hinders the refinement of individual temperature factors. Additionally, the relative electron densities of S_2 and S_3 positions (with respect to S_1) were refined. It can be appreciated that the values found are in a fairly good agreement with those in Tab. I in the main text.

II. SURFACE OXIDATION

Spectroscopic ellipsometry can be employed as an effective tool for the observation of time dependent changes on the sample surface which express themselves in surface optical properties that vary over time. Determination of optical constants relies heavily on the knowledge of sample's multilayer structure. Our thin layers of CuMnAs were exposed to air so that the presence of surface oxide layer may be expected. The following analysis led us to conclude that a few nanometres thick layer of cuprous oxide forms at a time scale of days. A freshly grown sample (20 nm thick CuMnAs layer on GaP) was put into the ellipsometer within two hours after being taken out from the MBE apparatus. A model structure assuming only the CuMnAs layer and surface roughness was used to fit experimental data as described in the main text resulting in the determination of optical parameters of CuMnAs.

Afterwards, the sample was exposed to air for about two weeks and the ellipsometric measurements were repeated several times during this time interval. The whole set of experimental data (i.e., for four different times of air exposure) was fitted at once with a modified model structure. This structure assumed another layer on top of CuMnAs. Only three thicknesses (l_{CuMnAs}, thickness of the additional layer l_o and surface roughness l_r) were left as fitting parameters. The best fit was obtained using optical parameters of Cu_2O and resulting thickness of this layer (l_o) was an increasing function of time elapsed from the

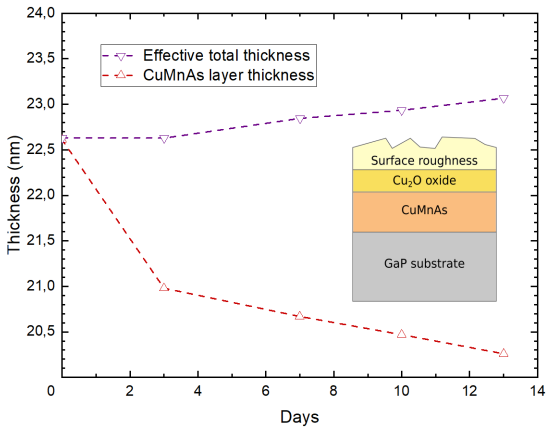

FIG. 2. After several days of air exposure (starting after the sample is taken out from MBE chamber), a thin oxide layer forms on the surface, gnawing at the actual material (CuMnAs). Nevertheless, the effective total thickness of the layer (see definition in the text) still slightly increases with time.

growth. Manganese and arsenic oxides yielded clearly worse fits. Since the surface roughness in the fit was treated as an effective layer containing 50% of air and 50% of the oxide, the total effective thickness was calculated as $l_{\mathrm{CuMnAs}} + l_o + \frac{1}{2} l_r$ and this quantity becomes larger in a matter of days, as shown in Fig. 2, and agrees very well (perhaps even surprisingly well) with the results of x-ray characterisation.

III. ORTHORHOMBIC SAMPLE

The imaginary part of permittivity shown by dashed line in Fig. 2 of the main text was measured on a bulk sample of CuMnAs grown using Bi flux similar to previously reported procedure[8,9] for the growth of $CuMn_3As_2$ and $Cu_2Mn_4As_3$. The elements with starting molar ratio Cu:Mn:As:Bi was 1:1:1:10 (1:1:1:15 also gives good results) were put into alumina crucibles (diameter 12 mm) and sealed under vacuum ($\sim 10^{-6}$ mbar) in quartz glass ampoules. The samples were slowly (2 °/min) heated up to 850 °C and kept at fixed temperature for 10 h. Then, they were slowly cooled down to 400 °C (3 °C/h) where the Bi flux was centrifuged. The single crystals were typically 1 to 3 mm long and 50 to 300 μm thick with the mass under 0.5 mg. The composition of the prepared single crystals was determined using energy dispersive x-ray (EDX) analysis.

Single crystals with composition $Cu_{34}Mn_{33}As_{33}$ were then subject of further studies. The

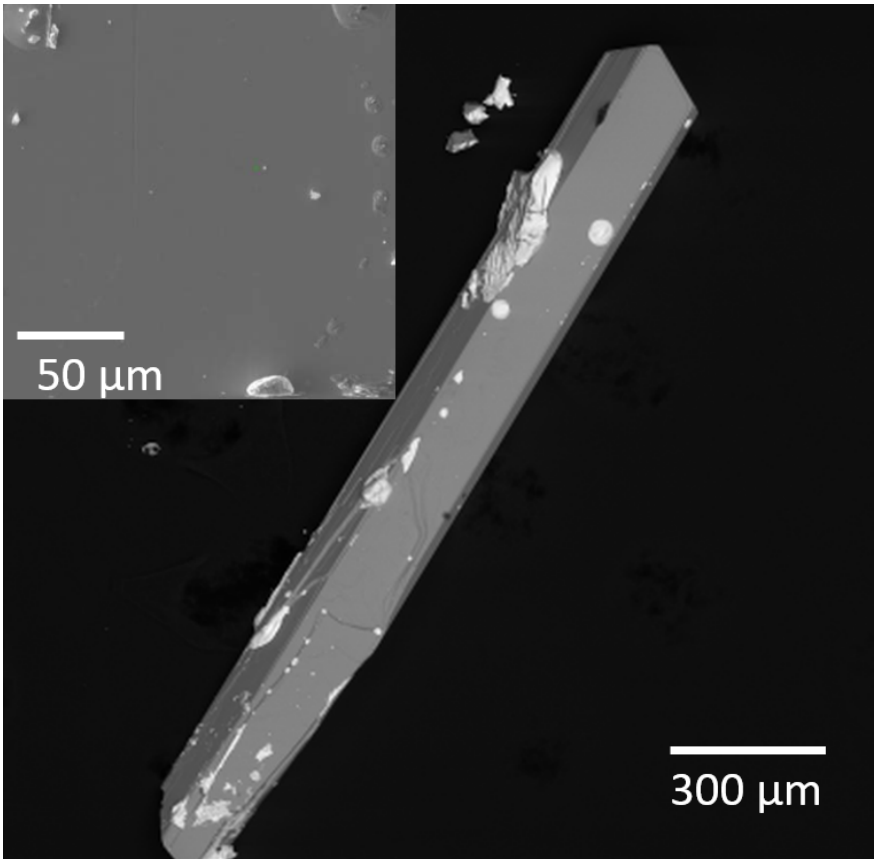

FIG. 3. Image of orthorhombic CuMnAs single crystals taken by SEM microscope. In BSE contrast, the remaining Bi flux droplets are bright and clearly visible. The inset shows detail (SE contrast) on the sample surface with a clean area suitable for ellipsometric measurements.

variation in composition in selected samples was under 0.5%. The crystal symmetry and lattice parameters were determined by single crystal x-ray diffraction (XRD) using Rigaku RAPID II with Mo-Kα radiation in transmission geometry. We have confirmed orthogonal structure (space group Pnma) with lattice parameters $a = 0.6598(4)$ nm, $b = 0.3861(4)$ nm and $c = 0.73015(1)$ nm. The lattice parameters and magnetic behaviour of prepared samples are in agreement with recently reported results on single crystals prepared by the same method.[9]

Typical orthorhombic CuMnAs single crystal is shown in Fig. 3. The remaining Bi flux does not wet the surface and forms small droplets. In preparation for ellipsometry measurements, we used fresh as grown surface (rather than etching and exposing the surface to water) and selected an area free of the bismuth droplets. Focused light beam with spot size 0.15 to 0.2 mm was used and the ellipsometry itself was performed by the same procedure

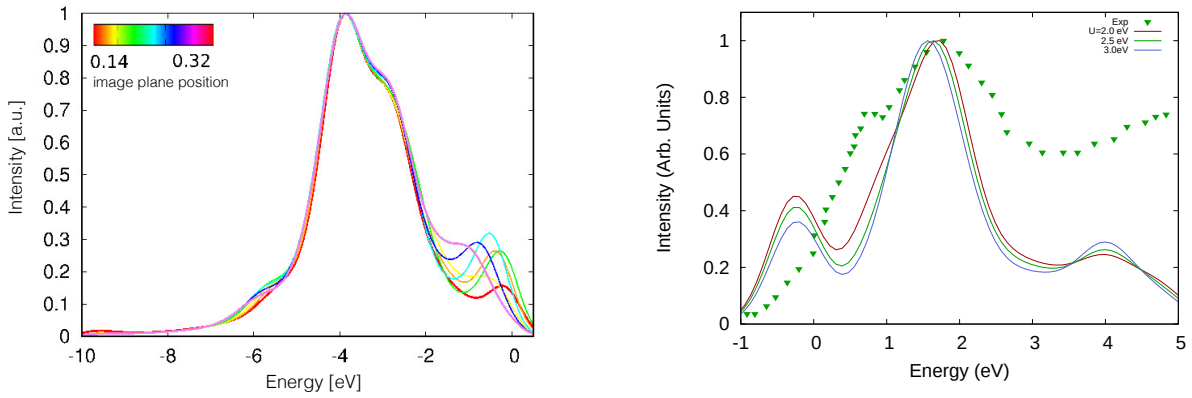

FIG. 4. *Left:* Result of one-step model of UPS ($U = 3$ eV) for different models of the surface barrier. *Right:* IPES measurement and modelling (RTP).

as for tetragonal films.

IV. UPS MODELLING AND IPES

In oder to describe photoemission spectra, we used the so called one-step model of photoemission. We used recently developed fully spin-density matrix formulation for the photocurrent[4] within the relativistic KorringaKohnRostoker (SPR-KKR) Green function method. As a first step of our PES investigations, we performed self-consistent LSDA+U ground state calculations for CuMnAs by means of SPR-KKR method. All parameters of the calcualtions has been as far as possible same as for the above mentioned LAPW based investigations and results obtained within SPR-KKR method are quantitativaly comparable to the LAPW method. The self consistent potentials and LSDA+U self energy are then used as an input for UPS and IPE investigations of CuMnAs(001) surface based on the formalism with k-vector integrated over the whole half-space.[10] As the LSDA+U does not include many-body finite life-time of the initial state this effect was included phenomenologically by imaginary part of potential (0.05 eV). The impurity scattering of the final state and its innelastic mean free path was modelled again by the imaginary part of the inner potential (2.0 eV) as usual.[3]

Additionally, for the photoemission calculations, we accounted for the surface barrier by use of a Rundgren-Malmström surface potential[5], which is included as an additional layer.

This procedure is described in for example in Ref. 6 and it accounts for the energetics and dispersion of all surface features. One of the most important parameters for this surface potential is the position of the classical image plane which in other words describes distance between surface barrier and last surface layer. In the left panel of Fig. 4, we show UPS spectra calculated for the position of the image plane in the range between $0.14c$ and $0.32c$. The spectral feature close to the Fermi level (B in Fig. 5 of the main text) clearly shows a strong surface character. On the other hand, the main peak at binding energy of -4 eV (feature A of Fig. 5) are bulk states with predominant Mn-character.

The conduction band electronic structure of the interfaces was studied by means of Inverse PhotoEmission Spectroscopy (IPES). Spectrum after integral background subtraction[7] is shown in the right panel of Fig. 4. The apparatus consists of an electron source based on a negative electron affinity GaAs photocathode coupled to an appropriate transport electron optics and a bandpass out-coming photons detector at fixed energy (9.3 eV) employing a KBr photocathode and a SrF_2 window. Like in the case of UPS, the Gaussian instrumental resolution broadening has been taken into account with FWHM = 0.8 eV (a conservative estimate[7]), evaluated measuring the IPES Fermi-edge of a monocrystalline Ag sample. In this case, the instrumental broadening is so high that it has not been necessary to consider the energy spreading due to lifetime effects. Agreement between experimental data and one-step model of photoemission is good, again there is one dominant peak (close to energy of 2 eV) which matches well the calculations whose dependence on Hubbard U is weaker than in the case of UPS. Spectral features below the energy of 1 eV are related to surface states.

---

[1] P. Wadley et al., J. Appl. Cryst. 46, 1749 (2013).

[2] U. Pietsch, V. Holý and T. Baumbach: High-Resolution X-Ray Scattering From Thin Films to Lateral Nanostructures, Springer 2004.

[3] J.B. Pendry, Low energy electron diffraction, Academic Press (1974).

[4] J Braun et al., New J Phys 16, 015005 (2014).

[5] G. Malmström and J. Rundgren, Computer Physics Comm. 19, 263 (1980).

[6] A. Nuber et al., Phys. Rev. B 83, 165401 (2011).

[7] M. Cantoni et al., Review of Scientific Instruments 70, 3572 (1999).

[8] K. Uhlířová et al., Journal of Alloys and Compounds 650, 224 (2015).

[9] Eve Emmanouilidou et al., Phys. Rev. B 96, 224405 (2017).

[10] J. Minár et al., Phys. Rev. B 63, 144421 (2001).